Bulletin of Mathematical Biology (2007) 69: 765–789
DOI 10.1007/s11538-006-9168-7

ORIGINAL ARTICLE

A Multidimensional Multispecies Continuum Model for Heterogeneous Biofilm Development

Erik Alpkvist[a,*], Isaac Klapper[b,c]

[a] *Applied Mathematics Group, School of Technology and Society, Malmö University, SE-205 06 Malmö, Sweden*
[b] *Department of Mathematical Sciences, Montana State University, Bozeman, MT 59717, USA*
[c] *Center for Biofilm Engineering, Montana State University, Bozeman, MT 59717, USA*

Received: 11 July 2005 / Accepted: 22 August 2006 / Published online: 9 January 2007

Abstract We propose a multidimensional continuum model for heterogeneous growth of biofilm systems with multiple species and multiple substrates. The new model provides a deterministic framework for the study of the interactions between several species and their effects on biofilm heterogeneity. It consists of a system of partial differential equations derived on the basis of conservation laws and reaction kinetics. The derivation and key assumptions are presented. The assumptions used are a combination of those used in the established one dimensional model, due to Wanner and Gujer, and for the viscous fluid model, of Dockery and Klapper. The work of Wanner and Gujer in particular has been extensively used through the years, and thus this new model is an extension to several spatial dimensions of an already proven working model. The model equations are solved using numerical techniques, for purposes of simulation and verification. The new model is applied to two different biofilm systems in several spatial dimensions, one of which is equivalent to a system originally studied by Wanner and Gujer. Dimensionless formulations for these two systems are given, and numerical simulation results with varying initial conditions are presented.

Keywords Biofilm · Continuum model · Mathematical modeling · Multidimensional · Multiple species

1. Introduction

Wild-type bacterial biofilms, that is, biofilms not grown in a laboratory environment, generally consist of many different species of bacteria. Different species

*Corresponding author.
E-mail addresses: erik.alpkvist@ts.mah.se (Erik Alpkvist), klapper@math.montana.edu (Isaac Klapper).

generally exhibit different growth and survival properties resulting in multidimensional heterogeneity. This heterogeneity is certainly a result of both external and internal influences. (Even in the single species case, heterogeneity may result from the presence of multiple biomass components or particulate substances, e.g., bacteria, extracellular polymeric substances (EPS), and inert biomass.) As an example, the work of James et al. (1995) has suggested that for a certain biofilm system the presence of mixed species affects the biofilm thickness. In particular, their work indicates that the presence of one species may enhance the growth of another. We consider here the multidimensional effects of multispecies, or multiple component ecology. Questions regarding biofilm ecology relevant to the morphology include the following: Do the interactions of the various biomass components affect the morphological shape of the biofilm? Conversely, does the morphology have an effect on interactions between different biofilm components? The answer to both of these questions is probably yes.

Continuum models capable of describing multispecies interactions are often based upon the work of Wanner and Gujer (1986), henceforth referred to as W-G. These models have aided tremendously in the understanding of the interactions of bacterial species in biofilms. Through the introduction of the commercialized software Aquasim, Reichert (1998), the W-G model has also served as an educational tool for engineers. However, biofilms were recognized to be morphologically heterogeneous materials during the early 1990s through studies using confocal laser scanning microscopy (CLSM). But W-G and many of its offshoots were pre-CLSM, and at that time spatial heterogeneity of biofilms was not taken into account or believed to be important. Thus, microbial and substrate distribution were only allowed to vary in the direction perpendicular to the substratum, resulting in models for one space dimension only. During 1990s, this deficit spawned attempts to capture the heterogeneous morphology within multidimensional multispecies biofilm models based on discrete biomass representations. The field of describing and characterizing experimental observations by these types of models is a growing one. Examples of discrete models which include multispecies effects are individual-based models (IBM) (e.g., Kreft et al. (2001), Kreft and Wimpenny (2001), Picioreanu et al. (2004), Xavier et al. (2004), Xavier et al. (2005)) and Cellular Automata (CA) based models (e.g., Noguera et al. (1999), Hunt et al. (2003)). The extension of discrete models such as the CA or IBM to several microbial species is usually straightforward. The local rules for the interactions between different species are often defined as in the single species models and the interactions are completely described by the individual species reaction kinetics. Computational results for these types of models include however an element of randomness since algorithms used to solve for biomass transport give rise to different outputs for the same initial condition. This randomness can be regarded as artificial—it arises from details in the algorithm rather than from the process modelled. Therefore, for a discrete model, several runs with the same initial state are needed to average the stochastic effect before conclusions are drawn. But due to the lack of a mathematical framework, there exists no a priori guidelines governing the number of runs for making a valid prediction within a given degree of certainty. These drawbacks are avoided by the use of continuum models with

simulations based upon accepted numerical methods with an existing error analysis. Such a framework boosts confidence in conclusions especially in several space dimensions.

Continuum models assume that concentrations of biomass may be adequately described by one or more density fields and, generally, that those density fields obey some sort of conservation law, e.g., conservation of mass or momentum. See, for example, the diffusion model by Eberl et al. (2001), Eberl (2004), the viscous fluid model, Dockery and Klapper (2001) (referred to here as the D-K model), the model of chemotactic colony growth Alpkvist et al. (2004a), or that by Cogan and Keener (2004). Small-scale details of an individual microorganism are not directly taken into account; rather it is assumed that a given property of interest, say, for example, the nutrient uptake rate, averages smoothly over groups of microorganisms. Thus, one source of (generally unmeasured and unparameterized) stochasticity, namely local individual variation, is eliminated. A continuum approach offers several benefits over the discrete counterparts—the governing laws of physics used in other more mathematically mature disciplines (such as fluid dynamics, solid mechanics, etc.) are naturally incorporated, and furthermore the uncontrolled random elements possessed by discrete models are removed. Continuum models are generally more difficult to derive and handle numerically, although from the computational point of view, continuum models have the advantage that such models generate deterministic solutions. Thus, only one computational run will be adequate for any given initial condition. From a mathematical point of view, the possibility for analytical study in order to characterize and compare model results also makes continuum models attractive, e.g., Overgaard (2006) or Efendiv et al. (2002).

While one-dimensional models like W-G have allowed inclusion of multiple species, a multidimensional multispecies continuum model of the W-G type has not yet been formulated. This work presents a new continuum approach for multispecies biofilm growth based upon a combination of those used for the W-G and D-K models. When applying the new model to a planar (i.e., flat) biofilm system, it reduces to a one-dimensional model equivalent to W-G. This is an important point since W-G has been extensively used and heavily tested, through the use of Aquasim, with good results.

The following issues are emphasized in this work:

- General model derivation with key assumptions.
- Application of the general model to two different biofilm systems.
- Numerical methods.
- Simulation results with conclusions.

The organization of this paper takes the following form: the next section treats the derivation and key assumptions of the model. Section 3 describes two biofilm systems to which the new model is applied. Section 4 briefly describes the computational techniques used. Computational results are presented in Section 5, and Section 6 presents the conclusions of this work.

2. Modeling

Consider a biofilm enclosed within an open subset Ω of R^3:

$$\Omega = \{\mathbf{x} = (x, y, z) : \ 0 < x < W, \ 0 < y < L, \ 0 < z < H\},$$

where W, L, and H denotes the width, length, and height of the domain.

The computational domain consists of two main phases at time t, the biomass region B_t and the liquid region $\Omega \backslash B_t$, see Fig. 2. There are two moving boundaries within Ω: the biomass–liquid interface defined by the curve Γ_t separating the biomass–liquid interface, and Γ_{H_b}, the bulk–liquid interface at a fixed height H_b above B_t. Let the top boundary of Ω be denoted by $\Gamma_H = \{\mathbf{x} : \ z = H\}$ and the bottom boundary by $\Gamma_B = \{\mathbf{x} : \ z = 0\}$. The biomass region B_t consists of N_b different components: bacterial species, EPS, and inert biomasses. We refer to these different components in the biofilm as either species or biomass phases. Also, through both the liquid and biomass regions, N_c different substrates are transported diffusively.

We assume that there is a distance from the biofilm at which fluid mixing is able to replenish or remove diffusive components faster than they are used or produced. The interface of this boundary layer region is Γ_{H_b}. The effects of biofilm structure on mass transfer in biofilm systems were experimentally investigated by Zhang and Bishop (1994) and Yang and Lewandowski (1995). The boundary layer has also been experimentally observed to depend on the structure of the biofilm, see Wäsche et al. (2002).

Within Ω, we impose *conservation of mass* on the biomass phases and substrates. Conservation of mass for the biomass phases yields

$$\frac{\partial b_i}{\partial t} + \nabla \cdot \mathbf{J}_i^b = g_i \quad \text{for } i = 1, \ldots, N_b \tag{1}$$

where the b_is and $\mathbf{J}_i^b$s are the concentrations and fluxes of the biomasses, respectively, and the g_is are the functions describing the gain or loss of the biomasses. Conservation of mass for the substrates yields

$$\frac{\partial c_j}{\partial t} + \nabla \cdot \mathbf{J}_j^c = r_j \quad \text{for } j = 1, \ldots, N_c, \tag{2}$$

where the c_js and the $\mathbf{J}_j^c$s are the concentrations and fluxes of substrates, respectively, and the r_js are functions describing gain or loss of substrate concentrations, i.e., how the substrates react with the biomass components. Substrate diffusive fluxes are assumed to be governed by *Fick's law*

$$\mathbf{J}_j^c = -D_j \nabla c_j \quad \text{for } j = 1, \ldots, N_c \tag{3}$$

where D_j are assumed to be constant substrate diffusivities. Substrates interact with the biomass through consumption or excretion.

Let $\vartheta_i = \vartheta_i(t, \mathbf{x})$ and $\rho_i = \rho_i(t, \mathbf{x})$ denote the volume fraction and the density (relative to volume fraction) of species i at time t and position $\mathbf{x}$, respectively. Then $b_i = \rho_i \vartheta_i$ for species i. Assume that the biomass phases can be regarded as incompressible, so that

$$\rho_i(t, \mathbf{x}) \equiv \rho_i^*, \quad \text{for all } \mathbf{x} \in B_t \text{ and } t \geq 0 \tag{4}$$

where ρ_i^* are positive constants. We also note the simplifying fact that transport of substrates by diffusion is several orders of magnitude faster than changes due to growth and advection, see Picioreanu et al. (1999) for time scales of biofilm processes. This will enable us to consider *quasi-steady states* for the substrate concentrations so that Eq. (2) take the forms (using (3))

$$-D_j \nabla^2 c_j = r_j \quad \text{for } j = 1, \ldots, N_c. \tag{5}$$

To differentiate between specific substrate reactions for a given biomass phase, we define

$$r_j = \sum_{i=1}^{N_b} r_{j,i}(c_1, \ldots, c_{N_c}, \vartheta_1, \ldots, \vartheta_{N_b}) \quad \text{for } j = 1, \ldots, N_c$$

such that $r_{j,i}$ describes the uptake rate of substrate j by species i. We constrain the volume fractions of biomass to sum to one, i.e.,

$$\sum_{i=1}^{N_b} \vartheta_i(t, \mathbf{x}) = 1 \quad \text{for all } \mathbf{x} \in B_t \text{ and } t \geq 0. \tag{6}$$

Transport of biomass is governed by an advective process with a volumetric flow $\mathbf{u} = \mathbf{u}(t, \mathbf{x})$ for all species. Biomass fluxes are thus given by

$$\mathbf{J}_i^b = \rho_i \vartheta_i \mathbf{u} \quad \text{for } i = 1, \ldots, N_b. \tag{7}$$

Assume that the volumetric flow follows Darcy's law

$$\mathbf{u} = -\lambda \nabla p, \tag{8}$$

where $p = p(t, \mathbf{x})$ is the pressure and $\lambda > 0$ the Darcy constant, see Klapper (2004) for a discussion. Equation (8) is the force balance equation and states that growth expansion pressure ∇p is balanced by frictional response $\lambda^{-1}\mathbf{u}$. Note that on long time scales biofilms behave as very viscous fluids with large viscosity relative to water, see Shaw et al. (1996). Since the viscosity of the bulk fluid is small compared to that of the biomass, only small pressure gradients are needed in $\Omega \backslash B_t$ in order for the flow in the bulk fluid to adapt to that of the biomass. Hence, we may assume the pressure to be constant in the bulk fluid and thus set $p = 0$ in $\Omega \backslash B_t$.

By conservation of mass for the biomass species,

$$\frac{\partial \vartheta_i}{\partial t} + \nabla \cdot (\mathbf{u}\vartheta_i) = \frac{1}{\rho_i^*} g_i(c_1, \ldots, c_{N_c}, \vartheta_1, \ldots, \vartheta_{N_b}) \quad \text{for } i = 1, \ldots, N_b, \tag{9}$$

where the explicit dependencies of the rates g_i on the biomass volume fractions ϑ_i describe for example growth and decay of biomass. Summing (9) over i, one obtains

$$\frac{\partial}{\partial t}\left(\sum_{i=1}^{N_b} \vartheta_i\right) + \nabla \cdot \left(\sum_{i=1}^{N_b} \mathbf{u}\vartheta_i\right) = \sum_{i=1}^{N_b} \frac{g_i}{\rho_i^*}.$$

Using (6) and substituting into (8), we see that the pressure satisfies

$$-\lambda \nabla^2 p = \sum_{i=1}^{N_b} \frac{g_i}{\rho_i^*} \quad \text{in } B_t. \tag{10}$$

Also, since $\nabla \cdot \mathbf{u} = \sum_{i=1}^{N_b} \frac{g_i}{\rho_i^*}$, the transport Eq. (9) may be rewritten as

$$\frac{\partial \vartheta_i}{\partial t} - \lambda \nabla p \cdot \nabla \vartheta_i = \frac{g_i}{\rho_i^*} - \vartheta_i \sum_{i=1}^{N_b} \frac{g_i}{\rho_i^*} \quad \text{for } i = 1, \ldots, N_b. \tag{11}$$

As a remark, observe from (10) that p is proportional to λ^{-1}. Hence, the term $\lambda \nabla p$ in (11) is independent of λ, i.e., the biomass volume fractions ϑ_i are independent of λ. Thus, it is possible to set $\lambda = 1$ without affecting the results.

2.1. Boundary conditions

The boundaries are shown in Fig. 2. We impose periodic boundary conditions on our computational domain by identifying $\{\mathbf{x} : x = 0\}$ with $\{\mathbf{x} : x = W\}$ and $\{\mathbf{x} : y = 0\}$ with $\{\mathbf{x} : y = L\}$. The substratum located at the bottom boundary Γ_B is impermeable to mass transfer, mathematically enforced by no-flux boundary conditions for the governing Eqs. (5), (10), and (11) along Γ_B. We will assume that at a constant height H_b above the biofilm, there exist large reservoirs of each substrate with concentrations c_j^* for all j. This condition is expressed mathematically by inhomogeneous Dirichlet conditions at the reservoir boundary for the substrate Eq. (5). For the biomass transport Eq. (11), we impose a no-flux boundary condition at Γ_H. Since no biomass will have time to advance so far, this boundary condition does not have an effect on the solution and is only forcomputational

purposes. On the moving interface Γ_t, substrate concentrations and fluxes are continuous.

2.2. Complete model

Together with the boundary conditions, the model is now completely described by the following set of $N_c + N_b + 1$ coupled partial differential equations: the N_c semilinear Poisson Eq. (5) for substrate concentrations, the linear Poisson Eq. (10) for pressure, and the N_b advection Eq. (11) for the biomass volume fractions. The complete model takes the following form:

$$\begin{cases} -D_j \nabla^2 c_j = r_j \quad \text{for } j = 1, \ldots, N_c, \\ c_j = c_j^* \text{ for } \mathbf{x} \in \Gamma_{H_b}, \quad \partial c_j / \partial z = 0 \text{ for } \mathbf{x} \in \Gamma_B, \\ -\nabla^2 p = \sum_{i=1}^{N_b} \dfrac{g_i}{\rho_i^*} \quad \text{in } B_t, \\ p = 0 \text{ for } \mathbf{x} \in \Gamma_t, \quad \partial p / \partial z = 0 \text{ for } \mathbf{x} \in \Gamma_B, \\ \dfrac{\partial \vartheta_i}{\partial t} - \nabla p \cdot \nabla \vartheta_i = \dfrac{g_i}{\rho_i^*} - \vartheta_i \displaystyle\sum_{i=1}^{N_b} \dfrac{g_i}{\rho_i^*}, \\ \partial \vartheta_i / \partial z = 0 \quad \text{for } \mathbf{x} \in \Gamma_B, \text{for } i = 1, \ldots, N_b, \end{cases} \tag{12}$$

together with the previously described periodic boundary conditions on the sides of Ω

3. Applications

3.1. Example 1: Active, inert biomass, and oxygen

The biomass in a natural biofilm consists of several components: active bacterial cells (several species), dead or inactive cells, and EPS. These components have different properties including their interactive properties with the surrounding diffusive components (substrates and waste-products). Generally, the inactive biomass, the EPS, and dead cells make up a considerable amount of the mass in a biofilm. In this application, we choose to distinguish between two types of biomass components; the active and the inactive biomass. By active biomass, we refer to the component involved in chemical reactions with oxygen and by inactive (or inert) all other material not explicitly affecting the oxygen concentration, e.g., quiescent cells and EPS. The example here is comparable to one-dimensional models such as that of Rittmann and Manem (1992).

The individual densities for the biomass components are taken to be the same: $\rho^* = \rho_1^* = \rho_2^*$, where 1 and 2 refer to active biomass and inert material,

respectively. Let the uptake rates of oxygen, denoted by c_1, be described by

$$r_{1,1}(c_1, \vartheta_1, \vartheta_2) = -\vartheta_1 \rho^* \frac{1}{Y} \frac{\mu c_1}{k_{O_2} + c_1}$$

$$r_{1,2}(c_1, \vartheta_1, \vartheta_2) = 0$$

where Y, μ, and k_{O_2} are the yield, the maximum growth rate, the inactivation rate, and the Monod saturation coefficient, respectively. The growth rates for the two species are given by

$$g_1(c_1, \vartheta_1, \vartheta_2) = \vartheta_1 \rho^* \left(\mu \frac{c_1}{k_{O_2} + c_1} - k_\mathrm{d} - k_\mathrm{i} \right)$$

$$g_2(c_1, \vartheta_1, \vartheta_2) = \vartheta_1 \rho^* k_\mathrm{i}$$

where k_i is an inactivation rate constant and k_d is a decay rate constant. k_i governs the speed at which the active biomass transforms into inert material and k_d the hydrolysis rate of active biomass into CO_2. The parameter k_i is assumed to be of order of magnitude of k_d, as by Pritchett (2000). Note that for this example we do not model or solve for the CO_2 concentration, as it is not of interest for biofilm development in this particular case.

For computational reasons, we introduce dimensionless variables for space and time by $\mathbf{X} = \mathbf{x}/H$ and $T = t/t_D$, where t_D is the number of seconds per day. Spatial scaling also applies to the subsets and moving boundaries but for cosmetic reasons, we do not apply new notations to them. The dimensionless pressure and substrate concentrations are set to be $P = (\lambda t_D p)/H^2$ and $S = c_1/c_1^*$ and dimensionless constants are $\Phi^2 = (H^2 \mu \rho^*)/(Y D c^*)$ (the Thiele modulus), $\xi_1 = t_D k_\mathrm{d}$, $\xi_2 = t_D k_\mathrm{i}$, $\Psi = \mu t_D$, and $K = k_{O_2}/c^*$. See Table 1 for dimensional parameters and constants. In the new variables and constants, the model is completely described

Table 1 Model parameters for example 1, order of magnitude of parameters from Picioreanu et al. (1998a) with assumed inactivation rate

Parameter	Symbol	Value	Physical unit
Physical system dimensions			
Length	L	300×10^{-6}	m
Height	H	300×10^{-6}	m
Boundary layer height	H_b	$0.125H$	m
Oxygen concentration (O_2)	c_1^*	4×10^{-3}	kg/m^3
Maximum growth rate	μ	10^{-5}	s^{-1}
Growth yield	Y	10^{-1}	–
Monod saturation constant	k	10^{-5}	kg/m^3
Decay rate	k_d	2×10^{-6}	s^{-1}
Inactivation rate	k_i	10^{-6} and 6×10^{-6}	s^{-1}
Biomass density	ρ^*	60	kg/m^3
Diffusion coefficient	D	2×10^{-9}	m^2/s

by the following system:

$$\begin{cases} -\nabla^2 S = -\vartheta_1 \dfrac{\phi^2 S}{K+S}, \qquad S = 1 \text{ for } \mathbf{x} \in \Gamma_{H_b}, \quad \partial S/\partial z = 0 \text{ for } \mathbf{X} \in \Gamma_B, \\ -\nabla^2 P = \vartheta_1 \dfrac{\Psi S}{K+S} - \vartheta_1 \xi_1 \qquad \text{for } \mathbf{X} \in B_t, \\ \quad P = 0 \text{ for } \mathbf{X} \in \Gamma_t, \quad \partial P/\partial Z = 0 \text{ for } \mathbf{X} \in \Gamma_B, \\ \dfrac{\partial \vartheta_1}{\partial T} - \nabla P \cdot \nabla \vartheta_1 = \vartheta_1 \left(\dfrac{\Psi S}{K+S} - (\xi_1 + \xi_2) - \vartheta_1 \left(\dfrac{\Psi S}{K+S} - \xi_1 \right) \right), \\ \dfrac{\partial \vartheta_2}{\partial T} - \nabla P \cdot \nabla \vartheta_2 = \vartheta_1 \xi_2 - \vartheta_2 \left(\vartheta_1 \dfrac{\Psi S}{K+S} - \vartheta_1 \xi_1 \right), \\ \quad \partial \vartheta_i/\partial Z = 0 \text{ for } \mathbf{X} \in \Gamma_B \text{ and } \partial \vartheta_i/\partial Z = 0 \text{ for } \mathbf{X} \in \Gamma_H, \quad \text{with } i = 1, 2 \end{cases} \tag{13}$$

with periodic boundary conditions imposed for all functions at the sides of Ω.

3.2. Example 2: Autotrophs, heterotrophs, inerts, acetate, ammonium, and oxygen

The second example, illustrating ecological interactions, describes three types of components within the biomass. The active biomass, the part interacting through mass transfer with the diffusive components, is now identified as being composed of two different groups of bacteria. As in example 1, we also introduce a third biomass component, inactive biomass, and refer to it simply as inert biomass. The active biomass is supposed to be consisting of heterotrophic and autotrophic bacteria. For ease we refer to these species simply as heterotrophs or autotrophs respectively. Heterotrophs are a family of bacteria utilizing organic substrate, say acetate, while the autotrophs utilize inorganic substrate, say ammonia. For both species, the growth process requires access to oxygen and, as is often the case, oxygen can be considered the limiting diffusive component in the system. The autotrophs and heterotrophs compete within Ω for oxygen and space: interaction is governed implicitly by oxygen consumption in the substrate Eq. (5) and by the space constraint (6). The main motivations for this example are two-fold: first, the same example was studied using W-G and second, it is also used as a benchmark problem comparing biofilm models, see Noguera and Picioreanu (2004). This example is also important for waste-water applications, as seen and described in Fig. 1.

Uptake and growth rates are given by the stoichiometry and rate laws from W-G. As in the previous example, it is assumed that the densities of biomasses are equal for all three species, i.e., $\rho^* = \rho_1^* = \rho_2^* = \rho_3^*$ with 1 referring to the heterotrophs, 2 the autotrophs and 3 the inert biomass. Let c_1 denote the concentration of acetate, c_2 the concentration of ammonium, and c_3 the concentration of oxygen. Uptake

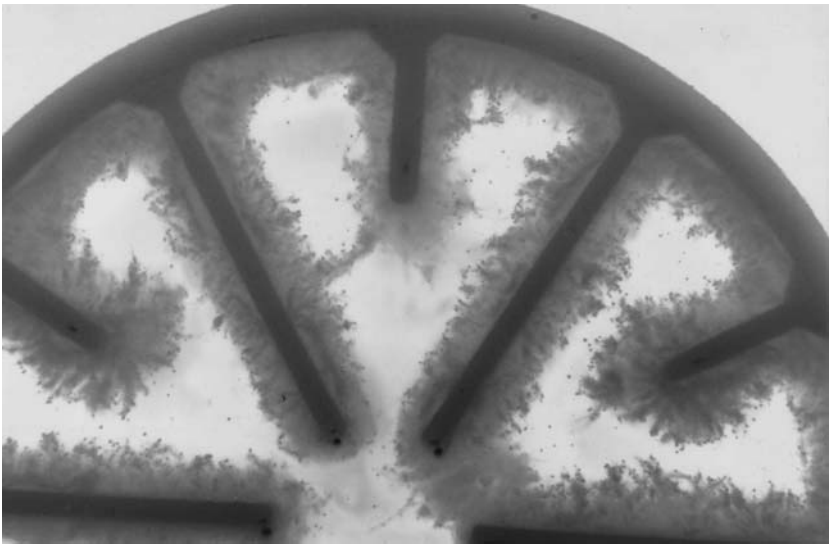

Fig. 1 A light-microscopy image of a multispecies biofilm growing on a part of a 20 mm in diameter biofilm carrier. Image taken by AnoxKaldnes AB (http://www.anoxkaldnes.com). *Black* is the carrier acting as substratum and *gray* the biomass. Biofilm carriers are engineered carriers, suspended and thoroughly mixed throughout the water phase in water treatment facilities. In the carrier the biofilm is protected. Generally, different biofilm carriers will exhibit different behaviors with respect to the bacterial composition and the conversion of different diffusive dissolved components. Carrier geometry is important for example in controlling mass transport properties within the carrier. For biofilms growing on carriers used in de-nitrifying water treatment, heterotrophic bacteria make treatment less effective by consuming the available oxygen and space on and around the carriers needed by the autotrophs. A simple system of this kind is described later as example 2 in Section 3.

rates for acetate are given by

$$r_{1,1} = -\frac{1}{Y_1}\mu_1\rho^*\vartheta_1\frac{c_3}{k_{O_1}+c_3}\frac{c_1}{k_{c_1}+c_1},$$
$$r_{1,2} = 0,$$
$$r_{1,3} = 0$$

and the uptake rates for ammonium are given by

$$r_{2,1} = 0,$$
$$r_{2,2} = -\frac{1}{Y_2}\mu_2\rho^*\vartheta_2\frac{c_3}{k_{O_2}+c_3}\frac{c_2}{k_{c_2}+c_2},$$
$$r_{2,3} = 0.$$

For the limiting substrate oxygen, the uptake rates are

$$r_{3,1} = -\frac{\alpha_1 - Y_1}{Y_1}\mu_1\rho^*\vartheta_1\frac{c_3}{k_{O_1}+c_3}\frac{c_1}{k_{c_1}+c_1} - b_1\rho^*\vartheta_1\frac{c_3}{k_{O_1}+c_3},$$

$$r_{3,2} = -\frac{\alpha_2 - Y_2}{Y_2}\mu_2\rho^*\vartheta_2\frac{c_3}{k_{O_2}+c_3}\frac{c_2}{k_{c_2}+c_2} - b_2\rho^*\vartheta_2\frac{c_3}{k_{O_2}+c_3}.$$

$$r_{3,3} = 0.$$

The growth rate for the heterotrophs is given by

$$g_1 = \mu_1\rho^*\vartheta_1\frac{c_3}{k_{O_1}+c_3}\frac{c_1}{k_{c_1}+c_1} - b_1\rho^*\vartheta_1\frac{c_3}{k_{O_1}+c_3} - k_1\rho^*\vartheta_1,$$

for the autotrophs

$$g_2 = \mu_2\rho^*\vartheta_2\frac{c_3}{k_{O_2}+c_3}\frac{c_2}{k_{c_2}+c_2} - b_2\rho^*\vartheta_2\frac{c_3}{k_{O_2}+c_3} - k_2\rho^*\vartheta_2,$$

and for the inert material

$$g_3 = k_1\rho^*\vartheta_1 + k_2\rho^*\vartheta_2.$$

Parameters and constants for this example are given in Table 2. Once again, introduce dimensionless variables $\mathbf{X} = \mathbf{x}/H$ and $T = t/t_D$ for space and time where t_D is the number of seconds per day. The dimensional free substrate concentrations are given by $S_1 = c_1/c_1^*$, $S_2 = c_2/c_2^*$, and $S_3 = c_3/c_3^*$. Within the substrate equations the dimensionless Thiele moduli are $\phi_{1,1}^2 = (H^2\mu_1\rho^*)/(Y_1D_1c_1^*)$, $\phi_{2,1}^2 = (H^2\mu_2\rho^*)/(Y_2D_2c_2^*)$, $\phi_{3,1}^2 = (H^2(\alpha_1 - Y_1)\mu_1\rho^*)/(Y_1D_3c_3^*)$, and $\phi_{3,2}^2 = (H^2(\alpha_2 - Y_2)\mu_2\rho^*)/(Y_2D_3c_3^*)$. The dimensionless Monod saturation constants are $K_{o_1} = k_{o_1}/c_3^*$, $K_{c_1} = k_{c_1}/c_1^*$, $K_{o_2} = k_{o_2}/c_3^*$, and $K_{c_2} = k_{c_2}/c_2^*$. Also denote $B_1 = (b_1\rho^*H^2)/(D_3c_3^*)$ and $B_2 = (b_2\rho^*H^2)/(D_3c_3^*)$. The substrate equations now take the form

$$\begin{aligned} -\nabla^2 S_1 &= \Sigma_1, \\ -\nabla^2 S_2 &= \Sigma_2, \\ -\nabla^2 S_3 &= \Sigma_3, \end{aligned} \tag{14}$$

where

$$\Sigma_1 = -\vartheta_1\phi_{1,1}^2\frac{S_3}{K_{o_1}+S_3}\frac{S_1}{K_{c_1}+S_1},$$

$$\Sigma_2 = -\vartheta_2\phi_{2,1}^2\frac{S_3}{K_{o_2}+S_3}\frac{S_2}{K_{c_2}+S_2},$$

$$\Sigma_3 = -\vartheta_1\left(\phi_{3,1}^2\frac{S_1}{K_{c_1}+S_1} - B_1\right)\frac{S_3}{K_{o_1}+S_3} - \vartheta_2\left(\phi_{3,2}^2\frac{S_2}{K_{c_2}+S_1} - B_2\right)\frac{S_3}{K_{o_2}+S_3}.$$

Dimensionless pressure is given by $P = (\lambda t_D p)/H^2$ with new dimensionless constants defined by $\Psi_{1,1} = \mu_1 t_D$, $\Psi_{1,2} = b_1 t_D$, $\Psi_{1,3} = k_1 t_D$, $\Psi_{2,1} = \mu_2 t_D$, $\Psi_{2,2} = b_2 t_D$, and $\Psi_{2,3} = k_2 t_D$. The pressure equation becomes

$$-\nabla^2 P = G \tag{15}$$

where $G = G_1 + G_2 + G_3$ and

$$G_1 = \vartheta_1 \left(\frac{S_3}{K_{o_1} + S_3} \left(\Psi_{1,1} \frac{S_1}{K_{c_1} + S_1} - \Psi_{1,2} \right) - \Psi_{1,3} \right),$$

$$G_2 = \vartheta_2 \left(\frac{S_3}{K_{o_2} + S_3} \left(\Psi_{2,1} \frac{S_2}{K_{c_2} + S_2} - \Psi_{2,2} \right) - \Psi_{2,3} \right),$$

$$G_3 = \vartheta_1 \Psi_{1,3} + \vartheta_2 \Psi_{2,3}.$$

Table 2 Model parameters used for example 2, with values taken from Wanner and Gujer (1986)

Parameter	Symbol	Value	Physical unit
Physical system dimensions			
Length	L	600×10^{-6}	m
Height	H	600×10^{-6}	m
Boundary layer height	H_b	0 and $0.4H$	m
Concentrations in bulk			
Acetate	c_1^*	3×10^{-3}	kg/m^3
Ammonium (NH_4^+)	c_2^*	13×10^{-3}	kg/m^3
Oxygen (O_2)	c_3^*	8×10^{-3} and 2×10^{-3}	kg/m^3
Diffusivity constants			
Acetate	D_1	9.6×10^{-10}	m^2/s
Ammonium (NH_4^+)	D_2	1.7×10^{-9}	m^2/s
Oxygen (O_2)	D_3	2.0×10^{-9}	m^2/s
Heterotrophs			
Maximum growth rate	μ_1	5.6×10^{-5}	s^{-1}
Substrate saturation constant	k_{c_1}	5×10^{-3}	kg/m^3
Oxygen saturation constant	k_{O_1}	5×10^{-3}	kg/m^3
Biomass yield	Y_1	4×10^{-1}	–
Endogenous rate constant	b_1	2.3×10^{-6}	s^{-1}
Inactivation rate constant	k_1	1.2×10^{-6}	s^{-1}
Conversion factor	α_1	1	–
Autotrophs			
Maximum growth rate	μ_2	1.1×10^{-5}	s^{-1}
Substrate saturation constant	k_{c_2}	1×10^{-3}	kg/m^3
Oxygen saturation constant	k_{O_2}	1×10^{-4}	kg/m^3
Biomass yield	Y_2	22×10^{-2}	–
Endogenous rate constant	b_2	5.8×10^{-7}	s^{-1}
Inactivation rate constant	k_2	1.2×10^{-6}	s^{-1}
Conversion factor	α_2	4.6	–

The transport equations for the biomass phases become

$$\frac{\partial \vartheta_i}{\partial T} - \nabla P \cdot \nabla \vartheta_i = G_i - \vartheta_i G \quad \text{for } i = 1, 2, 3. \tag{16}$$

The example is thus described completely by (14)–(16) together with boundary conditions as described previously.

4. Numerical methods

Numerical approximations for the governing equations are performed on a uniform fixed grid. We restrict ourselves to outlining the procedures in two spatial dimension, since the numerical techniques used extend straightforwardly to three spatial dimensions.

Let Ω denote an open connected rectangular subset of $\mathbf{R}^2$. Ω is associated with a uniform mesh of $[I \times J]$ points with mesh spacing h in each direction. Let the discrete numerical approximation on this mesh of a function $f = f(t, x, y)$ with $f : \mathbf{R} \times \Omega \to \mathbf{R}$ be denoted by $f^n_{i,j} = f(t_n, x_i, y_j)$. One important part of the numerical techniques used is the process of tracking a time-dependent domain $B_t \subset \Omega$. This is accomplished through the use of a level set framework with a level set function describing Γ_t, where Γ_t is the part of the boundary of B_t interior to Ω, see Fig. 2. See Osher and Fedkiw (2003) and Sethian (1999) for implementation details of the level set method. The level-set function $\phi = \phi(t, x, y)$ is defined to be a signed distance of $\mathbf{x} = (x, y)$ from the interface Γ_t. In particular, we have $\phi(t, \mathbf{x}) = 0$ for $\mathbf{x} \in \Gamma_t$. The time evolution of B_t is encoded by $t \to \phi(t, \cdot)$. We describe the motion

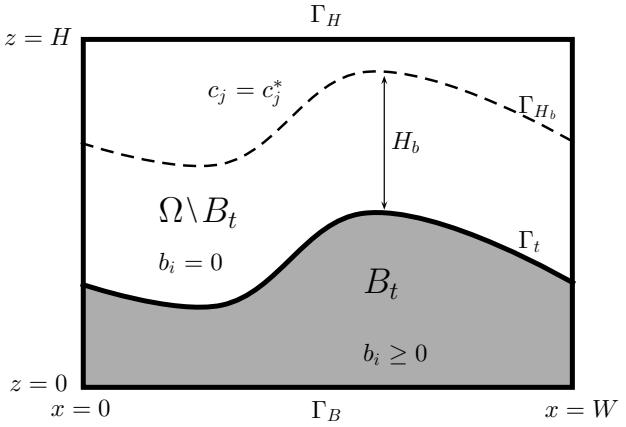

Fig. 2 Two-dimensional illustration of the domain Ω of height H and width W with subsets $\Omega \backslash B_t$ (liquid) and B_t (biomass) and moving boundaries Γ_t (biomass and liquid interface) and Γ_{H_b} (bulk–liquid interface). c_j and b_i are concentrations of substrates and biomasses, respectively. Note that we have $b_i = 0$ in $\Omega \backslash B_t$ and $c_j = c_j^*$ with c_j^* is a constant concentration of substrate in the bulk.

of a point $\mathbf{x} = \mathbf{x}(t)$ on the interface Γ_t by $\phi(t, \mathbf{x}(t)) = 0$ for all t. By differentiating with respect to time, we find that

$$0 = \nabla\phi(t, \mathbf{x}(t)) \cdot \mathbf{x}'(t) + \frac{\partial\phi}{\partial t}(t, \mathbf{x}(t)) \tag{17}$$

where $\mathbf{u}(t) = \mathbf{x}'(t)$ is the velocity under which the point $\mathbf{x}(t)$ is advected. Thus, the presented model includes nonlinear transport equations of the form

$$\frac{\partial\vartheta}{\partial t} + L(\vartheta, t) = f(\vartheta) \tag{18}$$

such as (17) (see also (11)). Here L, a spatial operator describing motion generated by an externally generated velocity field, takes the form

$$L(\vartheta, t) = \mathbf{u}(\mathbf{x}) \cdot \nabla\vartheta(t, \mathbf{x}). \tag{19}$$

where $\mathbf{u} = (u, v)$ is a velocity field with components u in the x-direction and v in the y-direction. The upwinding numerical approximation for this operator may be written as

$$\begin{aligned} L^n_{i,j} = {} & \max(u_{i,j}, 0) D^-_x \phi^n_{i,j} + \min(u_{i,j}, 0) D^+_x \phi^n_{i,j} \\ & + \max(v_{i,j}, 0) D^-_y \phi^n_{i,j} + \min(v_{i,j}, 0) D^+_y \phi^n_{i,j}, \end{aligned} \tag{20}$$

where $D^+_x\phi^n_{i,j}$, $D^-_x\phi^n_{i,j}$, $D^+_y\phi^n_{i,j}$, and $D^-_y\phi^n_{i,j}$ are forward $(+)$ and backward $(-)$ discrete operators. These spatial operators are discretized by a third order weighted essentially nonoscillatory (WENO) scheme, see Jiang and Peng (2000). Time discretization is performed using an explicit third order TVD-Runge–Kutta scheme as devised by Shu (1988). The functions ϑ described by the nonlinear hyperbolic Eq. (18) are not smooth at the sharp front Γ_t, introducing smearing in the numerical approximation around Γ_t. The velocity field describing the transport is $\mathbf{u} = 0$ in $\Omega\backslash B_t$. Thus, for a point at Γ_t travelling along a trajectory with a negative normal velocity in particular, the smearing will induce a loss of mass into $\Omega\backslash B_t$. This phenomena is somewhat suppressed using a suitable expansion of $\mathbf{u}$ into $\Omega\backslash B_T$ following a standard technique, see Chen et al. (1997). Determination of pressure as well as substrate utilization and diffusion within the model involves use of the Laplace operator ∇^2 (see (5) and (10)). For the D-K model, stability analysis has shown the importance of the depth of the active layer (the approximate depth to which substrate may substantially penetrate into the biofilm). It is important to realize that the function governing substrate concentration (5) is not twice differentiable at Γ_t in the classical sense. Thus, the numerical approximation of the Laplace operator at gridpoints close to this boundary has been based upon concepts similar to those in Liu et al. (2000). The symmetric ghostnode method of Gibou et al. (2002) is a second order accurate method for solving Poisson equations on irregular shaped domains on a uniform mesh. This method is used for discretizing the equation governing pressure (10) by generating a symmetric system of unknowns.

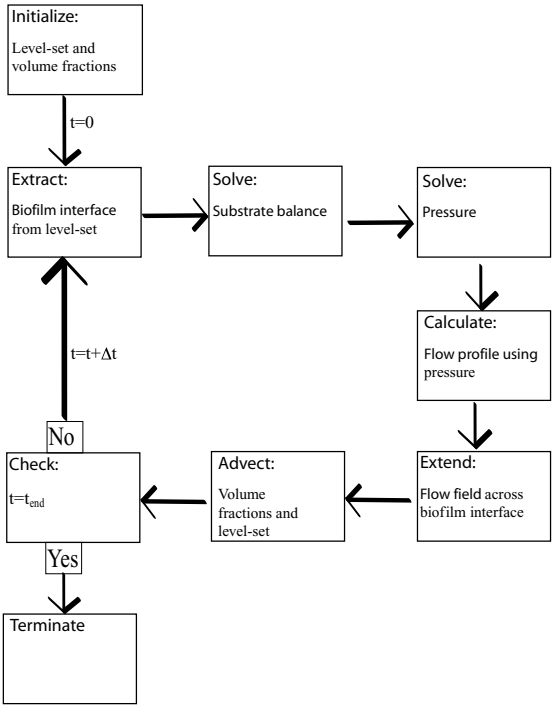

Fig. 3 Flowchart of the computational scheme.

A similar technique is also used for calculating the flow field given by (8) near the moving boundary Γ_t. For three spatial dimensions, the discrete systems for the substrates (5) and pressure (10) are very large systems and not feasible to solve using a direct method. Thus, the nonlinear FAS-multigrid method was applied and implemented, Hackbusch (1985). Refer to Fig. 3 for a flow-chart of the overall computational scheme. The code was tested and implemented for two and three spatial dimensions using C/C++ on a standard personal computer. Simulations in this paper have been performed on a 1-GHz Pentium III and computational time for the most demanding computation, i.e., the three spatial dimension computation on a $65 \times 65 \times 65$ grid, amounts to half an hour on this machine.

5. Results and discussion

We will begin by presenting simulation results for the simple biofilm system in example 1, see Section 3.1. These results will show that the interaction between the internal biomass components can have a large impact on the overall biofilm heterogeneity. We denote the two simulations presented as *e1-1* and *e1-2* respectively.

Simulation results for example 2, see Section 3.2, are presented in order to show model complexity and trends with respect to initial conditions. For this system, we present some typical results for both two and three spatial dimensions. We denote

the three simulations presented as *e2-1*, *e2-2*, and *e2-3* in their particular order of appearance.

The initial stage of biofilm formation starts with cells adhering to a surface coated by a protein film. Some of the simulations presented here, e.g., *e1-1*, *e1-2*, and *e2-1* are initially represented by perturbed interfaces. These kinds of initial conditions may be formulated explicitly and are thus reproducible. As a further example we also present the initial development of a biofilm with parameters set according to *e1-1* in Fig. 6 where the initial phase is described by a small number of cells adhering to the surface.

We may average over the volume fractions x and y by integration:

$$f_i(t, z) = \frac{\int_0^L \int_0^W \vartheta_i(t, x, y, z)\, \mathrm{d}x\, \mathrm{d}y}{WL} \qquad \text{for } i = 1, \ldots, N_b. \tag{21}$$

This representation is used to investigate the spatial distribution of the biomass volume fraction components along the z-dimension.

5.1. *Example 1*

The model applied to the biofilm system consisting of active and inert biomasses with oxygen was simulated with parameters given in Table 1. The biomass region was initially described at time $T = 0$ by

$$B_0 = \{\mathbf{X} \in \Omega;\ Y < 0.2 + 0.05 \sin(4\pi X)\}. \tag{22}$$

Within B_0, the initial volume fractions of active and inert biomass were given by

$$\begin{cases} \vartheta_1(0, \mathbf{X}) = 1 \\ \vartheta_2(0, \mathbf{X}) = 0 \end{cases}$$

for $\mathbf{X} \in B_0$.

Two representative sets of simulation runs for active and inert biomass are presented, first with the inactivation rate k_i set to $10^{-6}\,\mathrm{s}^{-1}$ and then second to $k_\mathrm{i} = 6 \times 10^{-6}\,\mathrm{s}^{-1}$, referred to as *e1-1* and *e1-2*, see Fig. 4 left and right columns, respectively. Note that the smaller value of k_i results in heterogeneity development; the large value of k_i suppresses interface heterogeneity. That is, for the higher inactivation rate, the simulations indicate that stability is enhanced, while an unstable interface develops for the lower inactivation rate. From the averaged distribution profiles shown in Fig. 5, observe that most of the active biomass is present near the biofilm interface. For *e1-1*, the larger amount of active biomass near the interface compared to that of *e1-2* will give rise to a shorter penetration depth of oxygen. Thus, a higher inactivation rate will increase the depth of the active layer by locally decreasing the amount of active biomass. (Linear stability results in D-K suggest that deeper active layers enhance homogeneity.) If so, then our results suggest that under some circumstances, growth-induced heterogeneity may be of lesser importance than commonly thought. That is, presence of inert material can

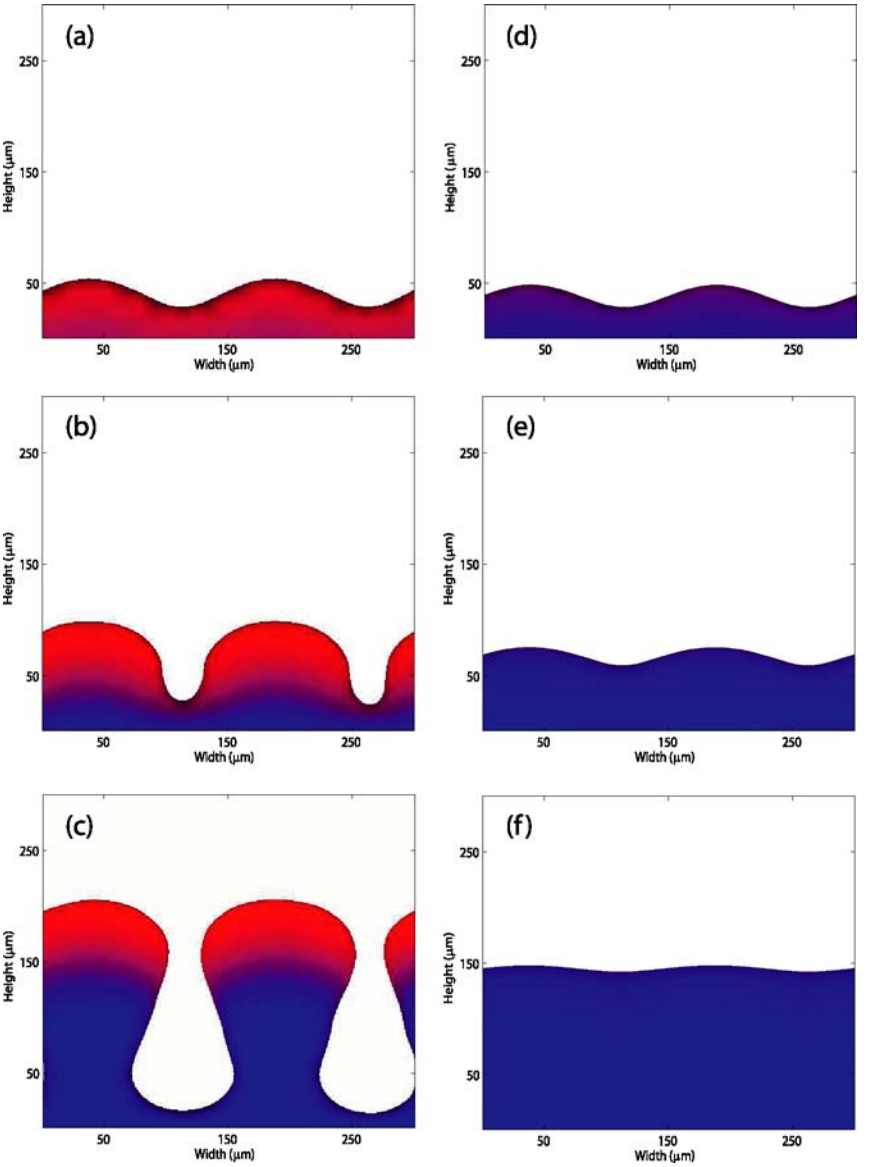

Fig. 4 Two two-dimensional simulations for the biofilm system described in example 1. The result of the simulation *e1-1* is shown in the left column, i.e., (a), (b) and (c). The result of the simulation *e1-2* is shown in the right column, i.e., (d), (e) and (f). Inactivation constants are $k_i = 10^{-6}$ and $k_i = 6 \times 10^{-6}$ for *e1-1* and *e1-2* respectively. Illustrations use the RGB channels where the *red* component represents active and *blue* the inert biomass. Time evolution from *top* to *bottom*: (a) $t = 3.8$, (b) $t = 16$, (c) $t = 41$ days for *e1-1* and (d) $t = 2.7$, (e) $t = 11.7$, (f) $t = 32.8$ days for *e1-2*.

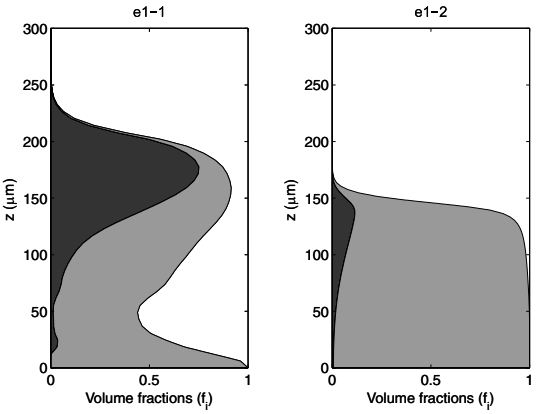

Fig. 5 Averaged volume fraction of *e1-1* and *e1-2* by (21) at times $t = 41$ and $t = 32$ days, respectively. *Black area* represents active biomass and light *gray* inert material.

suppress growth-induced heterogeneity. A further investigation of this observation might be possible using linear stability analysis.

The model is capable of a broad range of initial conditions. Figure 6 shows the early development of a simulation with a sparsely inoculated initial condition using the parameter set of *e1-1*.

5.2. Example 2

The biofilm system for heterotrophs, autotrophs, and inerts with limiting substrates oxygen, acetate, and ammonium was simulated with parameters given in Table 2. The competition for space between different species is solely dependent on the

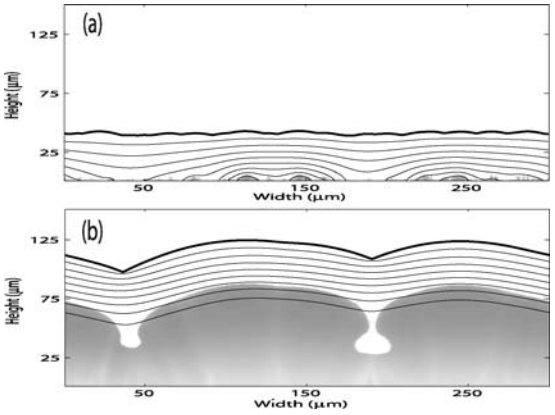

Fig. 6 Time evolution of sparsely inoculated initial condition at times $t = 0$ (a) and $t = 15.5$ (b). *Gray color* represents active biomass. *Contour lines* show oxygen profiles in the biomass and liquid. The *thick black line* is the boundary Γ_{H_b}.

growth and uptake rates of the diffusive components but is still complex. For a fast growing species, volume increase will utilize more substrate due to increased mass, often an advantage in an environment rich in oxygen and substrate. We will observe this in our computational results.

To illustrate the amount of internal spatial complexity the model may handle, the initial volume fractions were given a randomized initial distribution. We refer to this example by *e2-1*. The initial biomass region was described by

$$B_0 = \{\mathbf{X} \in \Omega;\ Y < 0.1 + 0.03\sin(4\pi X)\}. \tag{23}$$

The volume fractions ϑ_1, ϑ_2, and ϑ_3 were set randomly in space between 0 and 1 and subsequently smoothed a number of times by a Gaussian convolution operator in order to remove steep gradients. Time evolution for these initial conditions is shown in Fig. 7. Note that the biofilm components seem to grow along strains perpendicular to the substratum, visually similar to Fig. 1. This is the result of the largest vectorial component for pressure gradient acting along the direction perpendicular to substratum, thus flow of biomass is an order of magnitude smaller in the planes parallel to the substratum. This phenomenon is probably one of the main reasons why the one-dimensional models of W-G type work fairly well.

Single species biofilm models have been applied to explain and describe the phenomena of heterogeneous structure, i.e., the fingering behavior, see (cellular automata—Picioreanu et al. (1998b); continuum—Eberl et al. (2001); Klapper (2004); Overgaard and Alpkvist (2004); Alpkvist et al. (2004b)). These studies have shown that the *growth-limited* regime, i.e., high oxygen or substrate concentration, gives rise to a homogeneous biofilm structure whereas the *transport-limited* regime, i.e., low oxygen or substrate concentration, gives rise to fingering behavior. We will apply our multi-species continuum model to two such scenarios using the system in example 2.

Figure 8 represents a simulation referred to as *e2-2*. A number of colonies are constructed on the substratum. Initially, there exist both completely disjoint colonies made up of a single volume fraction as well as joint colonies made up of equal volume fractions of the two species. The oxygen concentration was set at $c_3^* = 8\,\mathrm{g/m^3}$ and the boundary layer thickness was set at $H_b = 0$, allowing biofilm to develop in an environment with an excess of oxygen, i.e., in a *growth-limited* regime. The simulation result is illustrated in the RGB channels with the red, green, and blue governing volume fraction of heterotrophs, autotrophs, and inert material, respectively. From the time evolution shown in Fig. 8, we can see the biofilm surface becoming more homogenous in time, as suggested by previous modeling studies for the *growth-limited* regime. Note also that colonies of different biomass phases remain separated, whereas colonies of the same phase completely merge.

Figure 9 shows the result of a three-dimensional computation, referred to as *e2-3*. Oxygen concentration and boundary layer height were set at $c_3^* = 2\,\mathrm{g/m^3}$ and $H_b = 0.4H$, respectively, resulting in a *transport-limited* regime for oxygen concentration. In Fig. 9(d), we observe a lower oxygen concentration around the heterotrophic colonies than around the autotrophic colonies, illustrating the fact that in this simulation $\phi_{3,1}^2 > \phi_{3,2}^2$, i.e., there is a faster uptake rate of oxygen for the

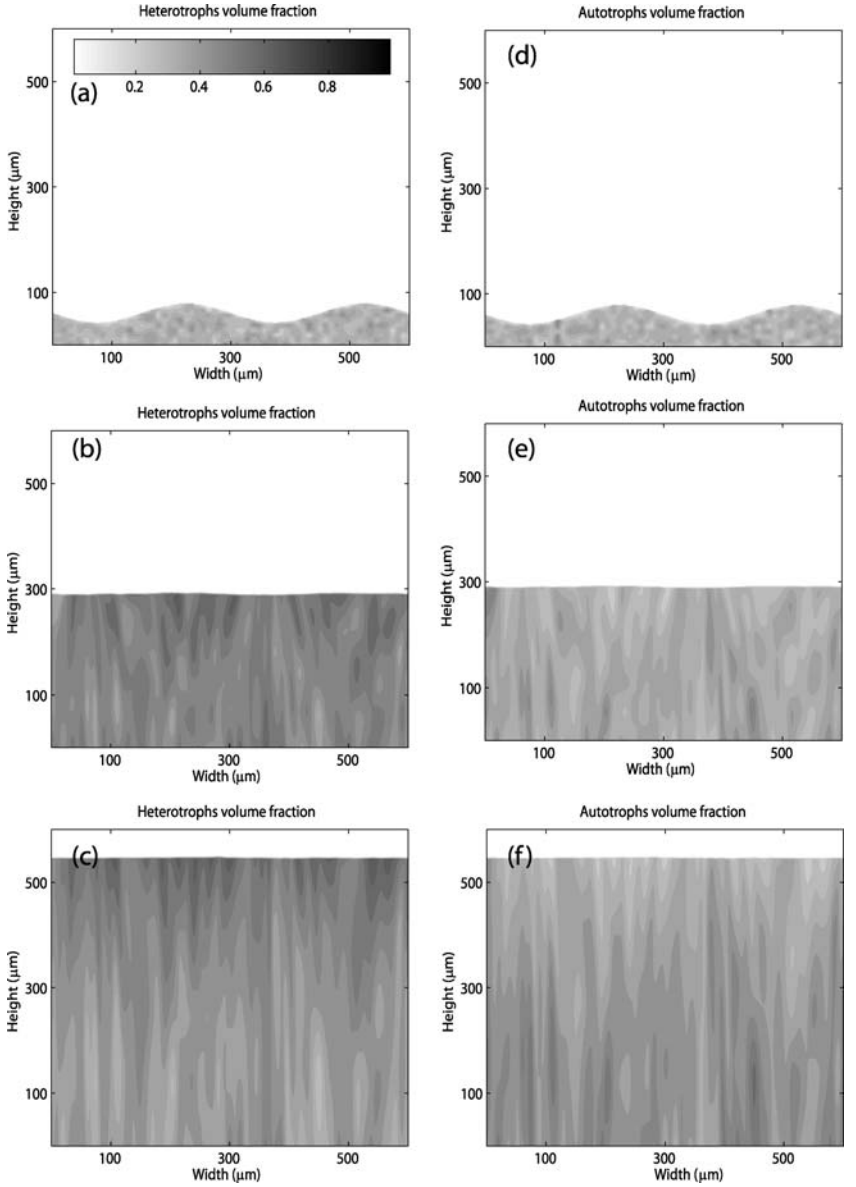

Fig. 7 Two-dimensional simulation denoted *e2-1*, for the biofilm system described in example 2 with an inhomogeneous initial condition. Volume fractions of heterotrophs and autotrophs are illustrated by filled isocontours. The left column (a), (b) and (c) shows the heterotrophs and the right column (d), (e) and (f) shows the autotrophs. Time evolution from *top* to *bottom*: (a) and (d) at $t = 0$, (b), and (e) at $t = 2.1$ days, (c) and (f) at $t = 3.1$ days.

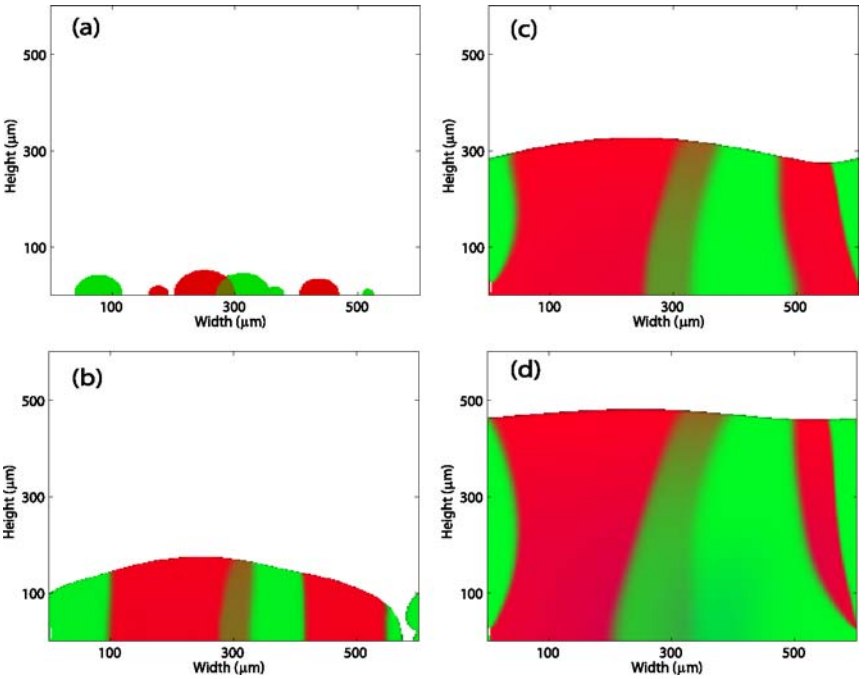

Fig. 8 Two-dimensional simulation denoted *e2-2* for the biofilm system described in example 2 with an initial condition described by joint and disjoint colonies of different species. Illustrations use the RGB channels where *red* represents the heterotrophs, *green* the autotrophs, and *blue* the inert biomass. Time evolution through *top left* (a) $t = 0$, *bottom left* (b) $t = 3.5$ days, *top right* (c) $t = 5.9$ days, and *bottom right* (d) $t = 7.8$ days.

heterotrophs than for the autotrophs. At the last step, Fig. 9(e), the autotrophs seem to have won the competition and the heterotrophs have been transformed into inert material. This is due to the fact that the oxygen needed by the heterotrophs for the reaction with acetate is greater than for process of autotrophs utilizing ammonium. Thus, the faster growing heterotrophs seem to be at a disadvantage in the *transport-limited* regime. This transformation process, for heterotrophs to inert material can be seen at the mid stage, Fig. 9(c), where the colonies of heterotrophs have become purple, i.e., degeneration into inert material is taking place.

The averaged distribution profiles for *e2-1* in Fig. 10 show trends similar to those in the computational results presented in W-G, with the heterotrophs starting to out-grow the autotrophs. For *e2-3*, on the other hand, the heterotrophs have almost completely converted to inert material, with a greater abundance of inerts near the bottom of the biofilm. Due to the heterogeneity of the biofilm surface, the total averaged mass fraction of the biofilm components do not add to 1 for *e2-3*. This is a multidimensional phenomenon that W-G is incapable of describing. The profile of *e2-2* is very similar to that of *e2-1*, even though the initial distributions are quite different.

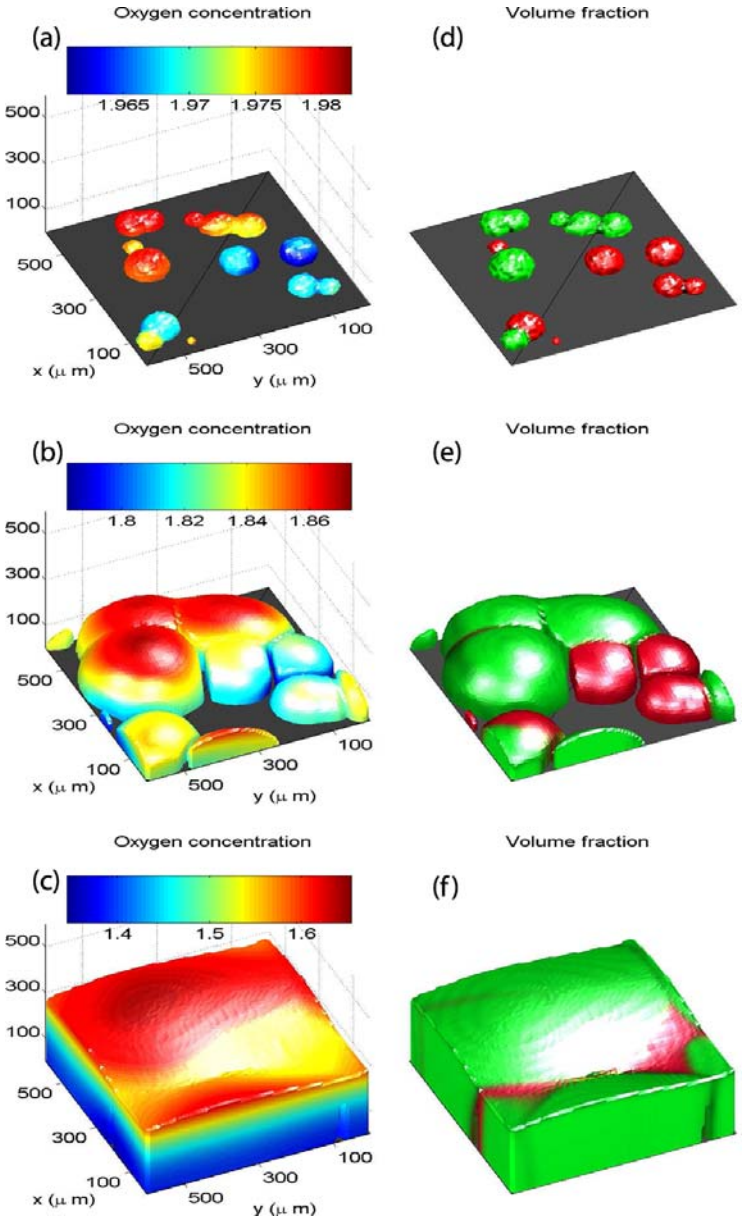

Fig. 9 Three-dimensional simulation denoted *e2-3*, for the biofilm system described in example 2 with initial conditions representing colonies. In the *left column* the biofilm surface is shown colored by the local oxygen concentration. In the *right column*, the different biomass components are shown using the RGB channels where *red* represents heterotrophs, *green* autotrophs, and *blue* inert biomass. Time evolution from *top* to *bottom* by (a) and (d) at $t = 0$ days, (b) and (e) at $t = 3.5$ days, (c) and (f) at $t = 5.1$ days.

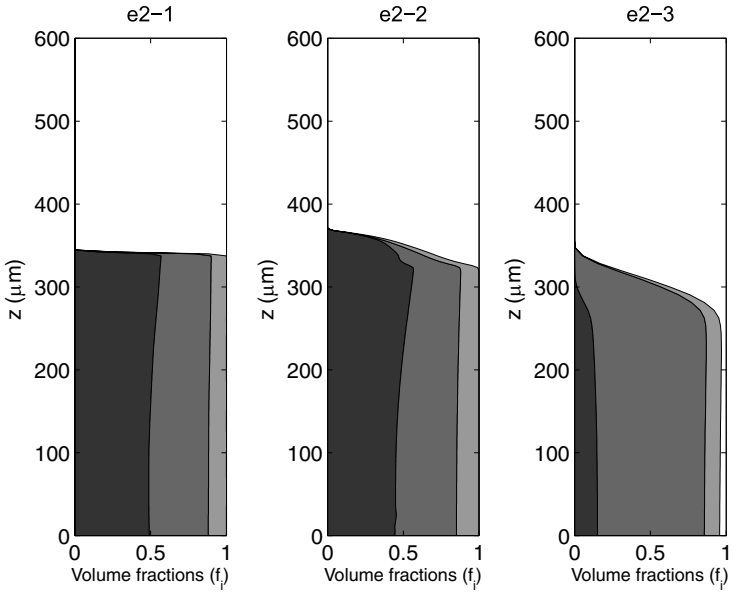

Fig. 10 Averaged volume fraction of *e2-1*, *e2-2*, and *e2-3* using (21), at times $t = 2.4$, $t = 6.4$, and $t = 5.2$ days. *Black area* represents the heterotrophs, *dark gray* the autotrophs, and *light gray* the inert materials.

6. Conclusions

A new continuum biofilm model has been proposed. The fundamental assumptions for this model are a combination of the ones presented for Dockery and Klapper (2001) and Wanner and Gujer (1986). Even for the two simple example systems, notable improvements and differences from these former models are apparent.

A number of steps have been taken to provide an adequate numerical approximation of the coupled nonlinear hyperbolic and elliptic systems describing the model. The numerical procedures have been tested and implemented for two possible biofilm systems. Representative simulations for these two systems have been presented in two and three spatial dimensions.

In the example with active and inert biomass the simulations suggest that the inactivation rate has an effect on the stability of the biofilm interface, a phenomenon not describable by a one-dimensional or one species model. This observation indeed shows that even for such a simple multiple component biofilm model, the internal mass balance interactions have a significant affect on the global biofilm structure. For the biofilm system describing competition between heterotrophic and autotrophic biomaterial, the results are in agreement with results from the one-dimensional model simulations of W-G.

Heterogeneous initial conditions and time evolution can be described and simulated using the presented model and computational framework. Such simulations represent biofilm systems for which a one-dimensional model is an inadequate

description or, conversely, under some circumstances verify adequacy of one dimensional representation. Thus, this extension, a generalization of one classical continuum model capable of describing and capturing heterogeneity in multiple spatial dimensions for multiple substrates and species, should be of use to biofilm modelers.

Acknowledgements

The authors would like to thank J. Dockery, N.C. Overgaard and C. Picioreanu for useful discussions and comments. I.K. was supported by NIH award 5R01GM067245-02 and E.A. acknowledges the financial support of the KK foundation and the scientific assistance of Dr. Magnus Christensson from AnoxKaldnes AB.

References

Alpkvist, E., Overgaard, N., Gustafsson, S., Heyden, A., 2004a. A new mathematical model for chemotactic bacterial colony growth. Wat. Sci. Tech. 49(11–12), 187–192.

Alpkvist, E., Overgaard, N., Heyden, A., 2004b. 3-D simulations and structural parameters for a continuum biofilm model. Proc. Biofilms 2004, Las Vegas, USA, 231–236.

Chen, S., Merriman, B., Osher, S., Smereka, P., 1997. A simple level set method for solving Stefan problems. J. Comp. Phys. 135(1), 8–29.

Cogan, N., Keener, J. P., 2004. The role of the biofilm matrix in structural development. Math. Med. and Biol. 21(2), 147–166.

Dockery, J., Klapper, I., 2001. Finger formation in biofilm layers. SIAM J. Appl. Math. 62(3), 853–869.

Eberl, H., 2004. A deterministic continuum model for the formation of EPS in heterogeneous biofilm architectures. Proc. Biofilms 2004, Las Vegas, USA, 237–242.

Eberl, H., Parker, D., van Loosdrecht, M., 2001. A new deterministic spatio-temporal continuum model for biofilm development. J. Theor. Med. 3(3), 161–175.

Efendiv, M., Eberl, H., Zelik, S., 2002. Existence and longtime behavior of solutions of a nonlinear reaction-diffusion system arising in the modeling of biofilms. Nonlinear Systems and Related Topics, 49–79, RIMS Tokyo.

Gibou, F., Fedkiw, R., Cheng, L. T., Kang, M., 2002. A second order accurate symmetric discretization of the Poisson equation on irregular domains. J. Comp. Phys. 176(1), 205–227.

Hackbusch, W., 1985. Multi-Grid Methods and Applications. New York: Springer-Verlag.

Hunt, S., Hamilton, M., Sears, J., Harkin, G., Reno, J., 2003. A computer investigation of chemically mediated detachment in bacterial biofilms. Microbiology 149(5), 1155–1163.

James, G., Beaudette, L., Costerton, J., 1995. Interspecies bacterial interactions in biofilms. J. Indust. Microbiol. 15, 257–262.

Jiang, G., Peng, D., 2000. Weighted ENO schemes for Hamilton-Jacobi equations. SIAM J. Sci. Comput. 21(6), 2126–2143.

Klapper, I., 2004. Effect of heterogeneous structure in mechanically unstressed biofilms on overall growth. Bull. Math Biol. 66(4), 809–824.

Kreft, J., Picioreanu, C., Wimpenny, J., Loosdrecht, M., 2001. Individual-based modelling of biofilms. Microbiology 147(11), 2897–2912.

Kreft, J., Wimpenny, J., 2001. Effect of eps on biofilm structure and function as revealed by an individual-based model of biofilm growth. Wat. Sci. Tech. 43(6), 135–141.

Liu, X.-D., Fedkiw, R., Kang, M., 2000. A boundary condition capturing method for Poisson's equation on irregular domains. J. Comp. Phys. 160(1), 151–178.

Noguera, D., Picioreanu, C., 2004. Results from the multi-species benchmark problem 3 (bm3) using two-dimensional models. Wat. Sci. Tech. 49(11–12), 169–176.

Noguera, D. R., Pizarro, G., Stahl, D. A., Rittman, B. E., 1999. Simulation of multispecies biofilm development in three dimensions. Wat. Sci. Tech. 39(7), 123–130.

Osher, S., Fedkiw, R., 2003. Level Set Methods and Dynamic Implicit Surfaces. Springer.

Overgaard, N., 2006. A moving-boundary problem related to a fluid model for biofilm growth. Submitted to Nonlinear Analysis, Theory, Methods & Applications.
Overgaard, N., Alpkvist, E., 2004. An investigation of Dockery-Klapper's biofilm model in the growth- and transport-limited extreme cases. Proc. Biofilms 2004, Las Vegas, USA, 236–241.
Picioreanu, C., Kreft, J., van Loosdrecht, M., 2004. Particle-based multidimensional multispecies biofilm model. Appl. Environ. Microbiol. 70(5), 3024–3040.
Picioreanu, C., van Loosdrecht, M., Heijnen, J., 1998a. Mathematical modeling of biofilm structure with a hybrid differential-discrete cellular automaton approach. Biotech. Bioeng. 58(1), 101–116.
Picioreanu, C., van Loosdrecht, M., Heijnen, J., 1998b. Mathematical modeling of biofilm structure with a hybrid differential-discrete cellular automaton approach. Biotech. Bioeng. 58(1), 101–116.
Picioreanu, C., van Loosdrecht, M., Heijnen, J., 1999. Discrete-differential modelling of biofilm structure. Wat. Sci. Tech. 39(7), 115–122.
Pritchett, L., 2000. Analysis of a one dimensional biofilm model. PhD thesis, Montana State University.
Reichert, P., 1998. Aquasim 2.0–computer program for the identification and simulation of aquatic systems. Tech. rep., Swiss Federal Institute for Environmental Science and Technolgy (EAWAG).
Rittmann, B., Manem, J., 1992. Development and experimental evaluation of a steady-state, multispecies biofilm model. Biotech. Bioeng. 39(9), 914–922.
Sethian, J., 1999. Level Set Methods and Fast Marching Methods, 2nd Edition. Cambridge University Press.
Shaw, T., Winston, M., Rupp, C., Klapper, I., Stoodley, P., 1996. Commonality of elastic relaxation times in biofilms. Phys. Rev. Lett. 93(9), 1–4.
Shu, C.-W., 1988. Total-variation-diminishing time discretization. SIAM J. Sci. Comput. 9(6), 1073–1084.
Wanner, O., Gujer, W., 1986. A multispecies biofilm model. Biotech. Bioeng. 28(33), 314–328.
Wäsche, S., Horn, H., Hempel, D., 2002. Influence of growth conditions on biofilm development and mass transfer at the bulk/biofilm interface. Wat. Sci. Tech. 36(19), 4775–4784.
Xavier, J., Picioreanu, C., van Loosdrecht, M., 2004. A modelling study of the activity and structure of biofilms in biological reactors. Biofilms 1(3), 377–391.
Xavier, J., Picioreanu, C., van Loosdrecht, M., 2005. A framework for multidimensional modelling of activity and structure of multispecies biofilms. Environ. Microbiol. 7(8), 1085–1103.
Yang, S., Lewandowski, Z., 1995. Measurement of local mass transfer coefficient in biofilms. Biotech. Bioeng. 48(66), 737–744.
Zhang, T. C., Bishop, P. L., 1994. Experimental determination of the dissolved oxygen boundary layer and mass transfer resistance near the fluid-biofilm interface. Wat. Sci. Tech. 30(11), 47–58.